

## ARTICLE

## OPEN



# Synthesis of UV-resistant and colorless polyimide films for optoelectrical applications

Le Xi<sup>1</sup>, Yadong Lv<sup>1</sup>✉, Jiabao Feng<sup>1</sup>, Yanyan Huang<sup>2</sup>, Yajiang Huang<sup>1</sup>, Qi Yang<sup>1</sup>, Guangxian Li<sup>1</sup> and Miqui Kong<sup>1</sup>✉

Due to their excellent mechanical properties and intrinsic flexibility, polyimides (PIs) are promising candidates for optoelectrical applications under harsh conditions such as flexible organic solar cells as well as flexible smart windows, etc. Much progress has been made on their optical transmittance; however, there remain significant concerns about their environmental stability, particularly their UV resistance. Herein, 4 types of colorless polyimides (CPIs) with different molecular structures containing trifluoromethyl, ethers, or fluorenes are carefully designed, and the dependence of their UV resistance on structures is explored systematically. It is found that the introduction of isopropylidene, ethers and fluorenes effectively enhances the UV resistance of CPI and its initial performance (optical transparency, thermal stability, and toughness) simultaneously as a result of the subtle manipulation of the conjugation structures. Specifically, the optimized polyimide film shows decent optical properties ( $T_{550\text{nm}} \sim 88\%$ , yellowness index  $\sim 3.26$ ), and thermal stability ( $T_{5\%} \sim 503^\circ\text{C}$  in  $\text{N}_2$  atmosphere,  $T_g \sim 312^\circ\text{C}$ ). Moreover, after high-intensity UV irradiation, CPI not only maintains over 90% of mechanical properties but also retains excellent optical properties ( $T_{550\text{nm}} \sim 88\%$ ) and thermal stability ( $T_{5\%} \sim 506^\circ\text{C}$ ). The design strategy paves the way for enhancing the durability of PIs for energy conversion and electronic applications resisting harsh conditions.

npj Materials Degradation (2024)8:6; <https://doi.org/10.1038/s41529-023-00422-w>

## INTRODUCTION

Aromatic polyimides (PIs) are well known for their superior flexibility as well as high thermal and mechanical properties originating from their rigid molecular structures and inter/intramolecular interactions<sup>1,2</sup>. Recently, the rapid advancement of optoelectrical applications such as flexible organic solar cells as well as flexible smart windows entails the development of colorless and optical transparent PIs<sup>3–6</sup>. These colorless polyimides (CPIs) also must maintain their physical and optical integrity under harsh operating conditions, especially high-intensity UV irradiation. As for the transparency consideration<sup>7</sup>, structural design approaches such as introducing asymmetric structure<sup>8</sup>, fluorine-containing group<sup>6</sup>, aliphatic<sup>9</sup>, and ether bonds<sup>10</sup> as well as electron-withdrawing groups have been proven to be efficient by minimizing or eliminating the formation of charge transfer complexes (CTCs). However, effective approaches to the simultaneous environmental stability, especially UV resistance, of transparent CPIs are still lacking.

It has been found that UV irradiation can severely deteriorate PIs<sup>11–16</sup>, which leads to the cleavage of chemical bonds, defects such as cracks, voids, and mass loss, and finally caused degradation of comprehensive properties and significantly reduced their lifetime. For example, Tanaka et al.<sup>16</sup> found that UV irradiation in air could cause oxidative cleavage of the imide ring followed by bridging between the polymer chains. In addition, Taniike et al.<sup>14</sup> investigated the photodegradation of the bio-derived polyimide and found that elongated radiation caused deterioration at the imide ring and the tertiary carbon of the cyclobutene ring with the growth of carbonyl species. Our previous work has shown that after UV irradiation, CPIs

experienced significant deterioration of mechanical properties and thermal stability, as well as the breakage of the ether bond, imide ring, and phenyl groups<sup>11,12</sup>. Recently, different methods for the enhancement of UV resistance of PIs were explored, including the incorporation of a light stabilizer/UV absorber in the bulk matrix<sup>17–20</sup> or protective coating on the surfaces<sup>21,22</sup>. Nevertheless, the migration of stabilizers from the matrix due to their low solubility or the delamination of coated materials can lead to significant deterioration of their UV protection ability. Alternatively, bulk structural design can be another promising strategy for the intrinsic enhancement of the UV resistance ability of CPIs. One of the most challenging issues is how to balance the optical transparency, UV resistance, and thermal stability to achieve excellent comprehensive properties. This is mainly because those goals contradict each other from the perspective of structural design, owing to the lack of a deep understanding of the quantitative structure-property relationship.

Herein, a facile strategy was utilized to synthesize a series of CPI films by introducing trifluoromethyl, fluorene, or ether groups. It is expected that those groups affect the electronic states in CPIs and the intra/inter charge transfer interactions, which determined the comprehensive properties of CPIs. The optical, thermal, mechanical, and especially UV resistance behaviors of the CPIs containing different structures were carefully studied and the underlying mechanisms were explored. It was found that with subtle manipulation of charge transfer interaction and the conjugation effects of CPIs, a balance between different key performances can be achieved. This work aims to provide deep insights and practical hints into the structural design strategies for high-performance CPIs toward optoelectrical applications under harsh conditions.

<sup>1</sup>College of Polymer Science and Engineering, State Key Laboratory of Polymer Materials Engineering of China, Sichuan University, Chengdu 610065, China. <sup>2</sup>School of Mechanical Engineering, Chengdu University, Chengdu 610000, China. <sup>3</sup>School of Aeronautics and Astronautics, State Key Laboratory of Polymer Materials Engineering of China, Sichuan University, Chengdu 610065, China. ✉email: yadonglv@scu.edu.cn; miquikong@scu.edu.cn

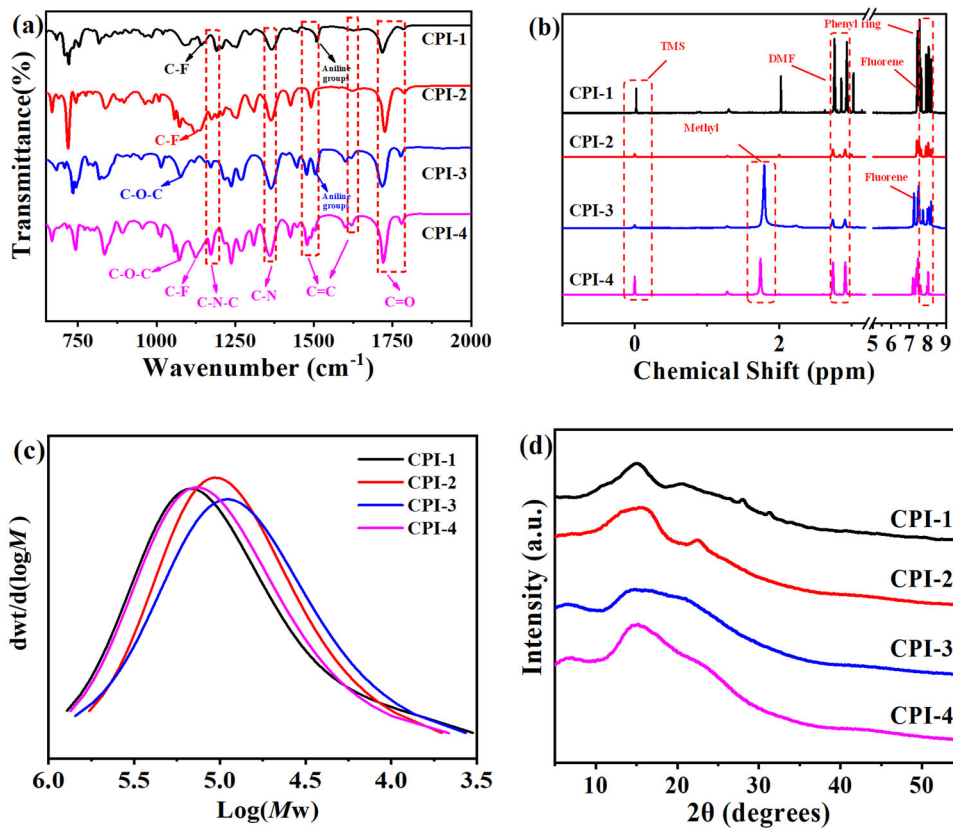


**Fig. 1 Structures of different CPI films. a** FTIR spectra, **b**  $^1\text{H}$ -NMR spectra, **c** molecular weight distribution curves, and **d** XRD curves of different CPI films.

## RESULTS AND DISCUSSION

### Synthesis and characterizations of CPI films

4 types of colorless polyimides (CPIs) films containing trifluoromethyl, fluorene, or ether groups, which were designated as CPI-1 to CPI-4 (6FDA-BAPF, 6FDA-TFMB, BPADA-BAPF, and BPADA-TFMB), were synthesized and characterized systematically. Different combinations of trifluoromethyl, fluorene, or ether groups were designed, aiming to control the charge transfer interactions between electron-donating diamine and electron-accepting dianhydride moieties. Figure 1a, b gave their molecular structures as measured by FTIR and NMR. As shown in Fig. 1a, the peak near  $1175\text{ cm}^{-1}$  corresponded to the deformation of the C-N-C in the imide ring, while peaks around  $1367\text{ cm}^{-1}$  corresponded to the axial stretching of the C-N bond<sup>12</sup>. Peaks near  $1475$  and  $1625\text{ cm}^{-1}$  were attributed to the stretching vibration of the C=C bond in the benzene ring, and the peaks near  $1781$  and  $1720\text{ cm}^{-1}$  corresponded to the stretching vibration of the C=O bond<sup>23</sup>. Those results clearly demonstrated the formation of imide ring structures. Specifically, for CPI-1, the stretching vibration of the C-F bond was observed at  $1140\text{ cm}^{-1}$ <sup>24</sup>, indicating the introduction of trifluoromethyl structures. For CPI-2, a significant peak of the C-F bond stretching vibration was observed near  $1122\text{ cm}^{-1}$  due to the introduction of hexafluorodiamine and hexafluorodianhydride structures. Peaks at  $1076$  and  $1236\text{ cm}^{-1}$  were observed in CPI-3 and CPI-4, which can be ascribed to the stretching vibration of the C-O-C bond<sup>10</sup>, indicating the presence of ether bonds in the aromatic ring structure. The successful introduction of trifluoromethyl structure can be proved by the appearance of the C-F bond stretching vibration peak at  $1124\text{ cm}^{-1}$  in CPI-4. Besides, Fig. 1b showed that peaks near  $1.79\text{ ppm}$  corresponded to  $-\text{CH}_3$  of the BPADA<sup>25</sup>. Peaks at  $2.7\text{ ppm}$  and  $2.9\text{ ppm}$  corresponded to DMF. Peaks around  $7.2$ – $7.5\text{ ppm}$

were ascribed to H of the fluorene<sup>26</sup>, and peaks of TFMB were around  $7.62$ – $7.64\text{ ppm}$ <sup>27</sup>. Moreover, peaks around  $8$ – $8.1\text{ ppm}$  corresponded to H in the 6FDA benzene ring<sup>27</sup>. In addition, Fig. 1c exhibited the molecular weight distribution curves of CPI films.  $M_w$  of CPI films ranged from  $120000$  to  $160000$ , which was in the typical range of CPIs. Moreover, all CPI films were basically amorphous (Fig. 1d), as the arrangement of the molecular chains was disrupted by the dense aromatic structure and large asymmetric groups<sup>1,2</sup>. These results together confirmed the designed chemical structures of CPIs.

To get a deep understanding of the conjugation effects of different CPI films, density functional theory simulation was used to theoretically calculate molecular orbital energies of different structures, as shown in Fig. 2. The balls with gray, white, red, blue, and light blue represented C, H, O, N, and F atoms, respectively. In addition, in the highest occupied molecular orbital (HOMO) and the lowest unoccupied molecular orbital (LUMO), the red part of the molecular structure represented the positive phase part, and the green part represented the negative phase part.  $E_{\text{LUMO}}$  was used to measure the electron-accepting ability of dianhydride; the larger the value of  $E_{\text{LUMO}}$ , the stronger ability of accepting electrons of dianhydride.  $E_{\text{HOMO}}$  was used to represent the electron-donating ability of diamine and larger  $E_{\text{HOMO}}$  reflected stronger electron-donating ability of diamine. The  $E_{\text{LUMO}}$  values of CPI-1, CPI-2, CPI-3, CPI-4, and traditional yellow PI film were calculated to be  $-2.87\text{ eV}$ ,  $-3.08\text{ eV}$ ,  $-2.38\text{ eV}$ ,  $-2.53\text{ eV}$ , and  $-3.43\text{ eV}$ , respectively. The  $E_{\text{HOMO}}$  values of CPI-1, CPI-2, CPI-3, CPI-4, and traditional yellow PI film were  $-6.07\text{ eV}$ ,  $-7.11\text{ eV}$ ,  $-5.95\text{ eV}$ ,  $-6.76\text{ eV}$ , and  $-6.29\text{ eV}$ , respectively. Energy band gap ( $\Delta E_{\text{gap}}$ ) was further calculated to evaluate the charge transfer interactions, which was related to the color of CPI films directly. It was accepted that the order of calculated band gaps was approximately parallel to that of absorption edge wavelengths of the experimental

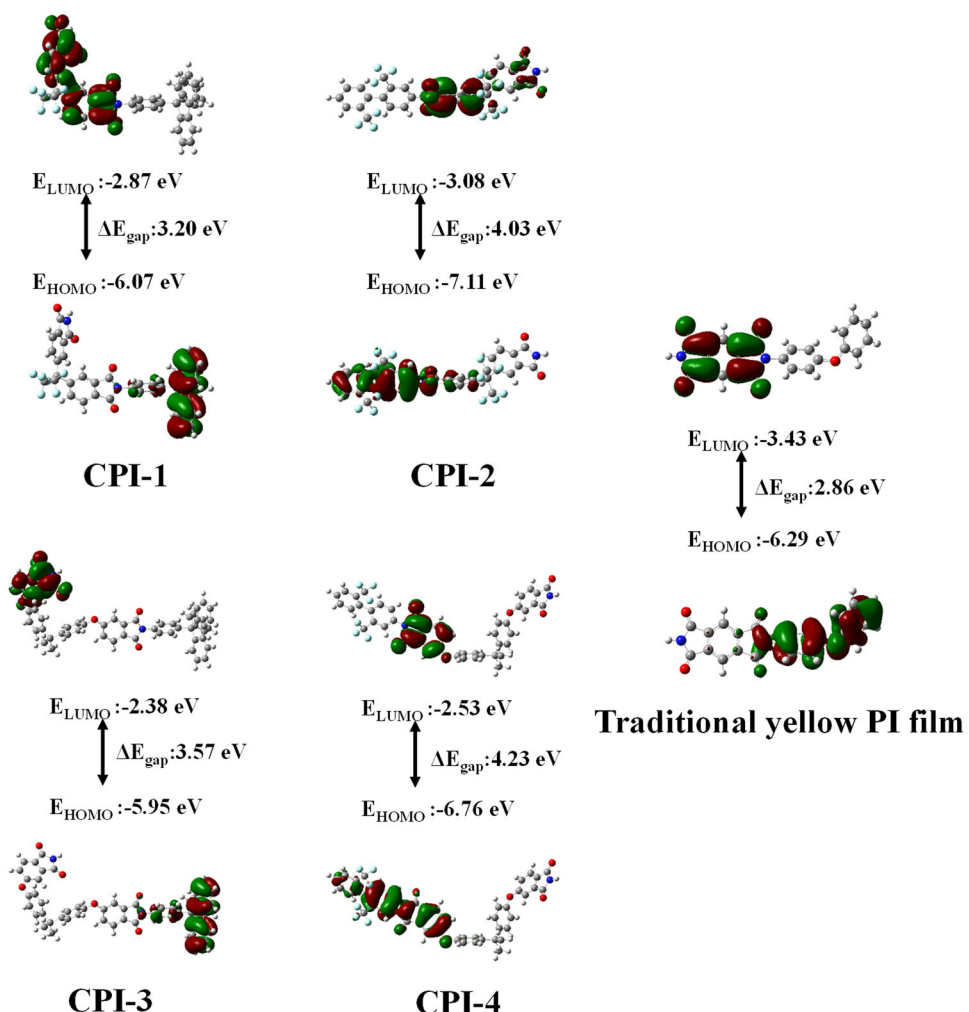


**Fig. 2** Molecular orbital energy of 4 types of CPI films and traditional yellow PI film.

spectra<sup>28</sup>.  $\Delta E_{\text{gap}}$  of CPI-1, CPI-2, CPI-3, CPI-4, and traditional yellow PI film were 3.20 eV, 4.03 eV, 3.57 eV, 4.23 eV, and 2.86 eV respectively. The results showed that the  $\Delta E_{\text{gap}}$  of all CPI films was significantly higher than that of traditional yellow PI film, and they were quite different. Note that DFT calculation only can quantitatively picture the light absorption of PIs, while more quantitative theoretical predictions needed additional correction by considering effects from the condensed phase<sup>28</sup>. Overall, the charge transfer interactions can be tuned in a wide range by the introduction of trifluoromethyl, ether bond, or fluorene groups, which made it feasible to balance different properties to achieve excellent comprehensive performance.

#### Initial performance of CPI films

Figure 3a showed the UV-Vis transmittance spectra and yellowness index (YI) of CPI films. All CPI films exhibited outstanding transmittance ( $T_{550\text{nm}} > 88\%$ ) and relatively low YI (<5.9). This result arose from the well-chosen diamines and dianhydrides, which changed the electron cloud distribution and reduced CTCs within their molecular chains<sup>29,30</sup>. The YI of CPI films followed the order: CPI-1 > CPI-3 > CPI-4 ≈ CPI-2. Further comparison of the overall optical properties of CPI films with that reported in the literature was carried out by employing Ashby plots (Fig. 3b).  $T_{550\text{nm}}$  and YI were represented in x and y-axes, respectively. Data points located in the right corner represented the best comprehensive optical properties. CPI films synthesized in this work possessed excellent

overall optical performance, which was comparable to that in the literature<sup>31–35</sup> and superior to that of representative traditional yellow PI films<sup>36,37</sup>.

Crucial mechanical and thermal performances that determined the applicability of CPI films in photoelectric fields were further compared, as shown in Fig. 4. The tensile strength of CPI films were 111.3 MPa, 94.4 MPa, 94.6 MPa, and 99.9 MPa, respectively, and Young's modulus were 2.7 GPa, 3.5 GPa, 2.3 GPa, and 2.4 GPa respectively, as shown in Fig. 4a. The high molecular weight of the synthesized films and aromaticity density might account for their excellent mechanical properties. Compared with CPI-3 and CPI-4, the higher Young's modulus of CPI-1 and CPI-2 could be mainly attributed to their more rigid skeletal structures<sup>10,38</sup>. The elongation at break of CPI films were 8.7, 4.7, 11.9, and 48.7%, respectively. Compared with CPI-3 and CPI-4, CPI-1 and CPI-2 exhibited lower elongation at break due to their high aromaticity density, resulting in brittle behavior. In contrast, ether bonds introduced into CPI-3 and CPI-4 contributed to enhancing the flexibility of molecular chains, resulting in a higher elongation at break<sup>10</sup>. Overall, CPI-3 and CPI-4 exhibited decent comprehensive mechanical properties with a balance of strength-ductility as a result of synergistic effects of ether bond, fluorene, or trifluoromethyl structure<sup>39</sup>.

The thermal degradation mechanism of polyimide mainly involved the cleavage of molecular chains, producing volatile products such as carbon monoxide, carbon dioxide, and carbonized benzene rings and leading to weight loss (Fig. 4b).

Furthermore, two distinct weight loss stages were observed in derivative thermogravimetric curves for CPI-1 and CPI-2 (Fig. 4c). The first stage, occurring around 550 °C, was mainly attributed to the thermal cleavage of C-N bonds or C-C bonds, resulting in the opening of imide rings. Then, active free radicals and small molecule gases such as CO and CO<sub>2</sub> could be generated under higher temperature conditions<sup>40</sup>. The second stage, occurring at temperatures greater than 620 °C, exhibited a gradually slowing weight loss rate due to the carbonization process of pyrolytic dehydrogenation of the benzene ring<sup>40–42</sup>. However, for CPI-3 and CPI-4, obvious weight loss occurred at a much lower decomposition temperature around 530 °C, presumably due to the decomposition of C-O-C, which has much worse decomposition stability and was easier to break<sup>43</sup>. It was found that the onset decomposition temperature ( $T_{5\%}$ ) and temperatures of the maximal rate of weight loss ( $T_{max}$ ) of CPI-3 and CPI-4 were lower than that of CPI-1 and CPI-2 (Fig. 4d, e). In addition, all CPI films

possessed a relatively high  $T_g$  (Fig. 4f), with values of 412, 359, 312, and 255 °C for CPI-1 ~ CPI-4 respectively. The relatively higher  $T_g$  of CPI-1 and CPI-2 can be attributed to the increase in the spatial barrier and the increase in molecular chain rigidity<sup>30,44,45</sup>, while the introduction of ether bond lowered  $T_g$  of CPI-3 and CPI-4 due to the increase in the flexibility of the material and the reduction of the energy barrier for chain movement.

### UV resistance of CPI films

The harsh working environments of optoelectrical applications, especially under high UV irradiation, presented a great challenge for CPI films. To this end, we further investigated the UV stability of CPI films with different structures by monitoring the effects of UV irradiation on their key properties. Effects of UV irradiation on the optical properties were monitored by UV-Vis spectra and YI, as shown in Fig. 5. An obvious enhancement of the absorption

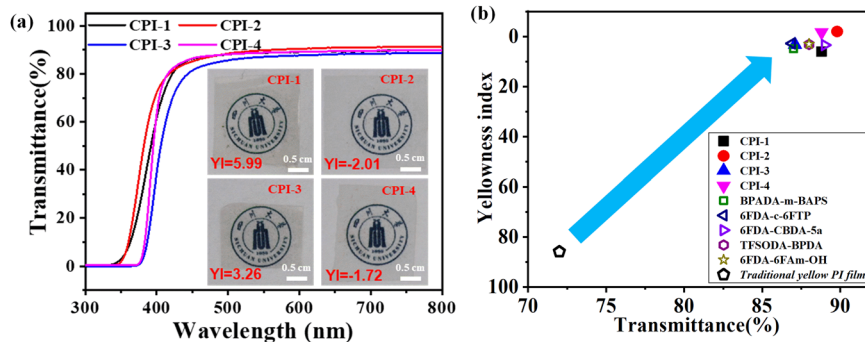


**Fig. 3 Transparency of different CPI films.** **a** UV-Vis transmittance spectra and YI of CPI films and **b** comparison of the overall optical performance (Ashby plot using the YI and  $T_{550\text{nm}}$ ) of CPI films in this work, as well as BPADA-m-BAPS<sup>31</sup>, 6FDA-c-6FTP<sup>32</sup>, 6FDA-CBDA-5a<sup>33</sup>, TFSODA-BPDA<sup>34</sup>, 6FDA-6Fam-OH<sup>35</sup>, and traditional yellow PI film<sup>36,37</sup> reported in the literature. m-BAPS Bis[4-(3-aminophenoxy) phenyl] sulfone, c-6FTP Aromatic triphenylenediamine monomers containing -CF<sub>3</sub>, CBDA-5a Cyclobutane-1,2,3,4-tetracarboxylic acid dianhydride and a new isomeric monomer containing a spiro ring and a benzodiazole ring, TFSODA 2,2'-bis(trifluoro-methyl)-4,4'-diamino diphenyl sulfoxide, BPDA 3, 3', 4, 4' -biphenyl dianhydride, 6FAm-OH 2,2-bis(3-amino-4-hydroxyphenyl) hexafluoropropane.

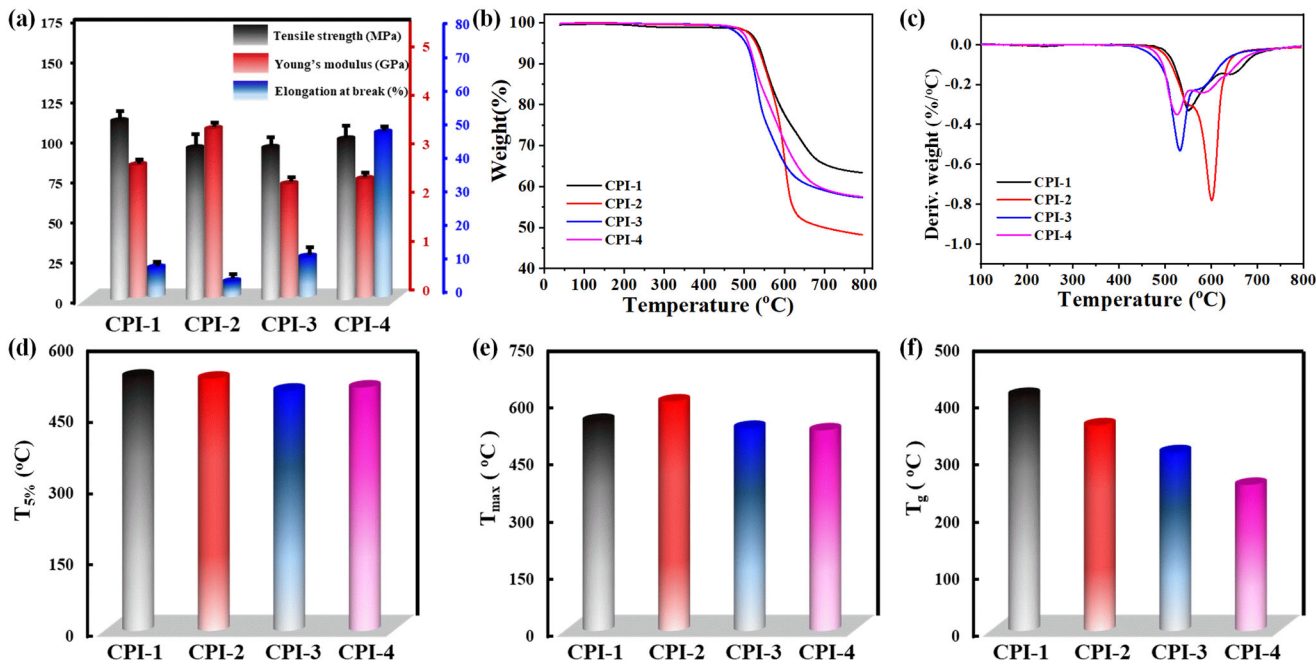


**Fig. 4 Mechanical and thermal properties of different CPI films.** **a** Mechanical properties, **b** thermogravimetric curves, **c** derivative thermogravimetric curves, **d** initial decomposition temperature ( $T_{5\%}$ ), **e** maximum decomposition temperature ( $T_{max}$ ), and **f** glass transition temperature ( $T_g$ ) of different CPI films. Error bars represent standard deviations from the results obtained at 3 replicated samples.

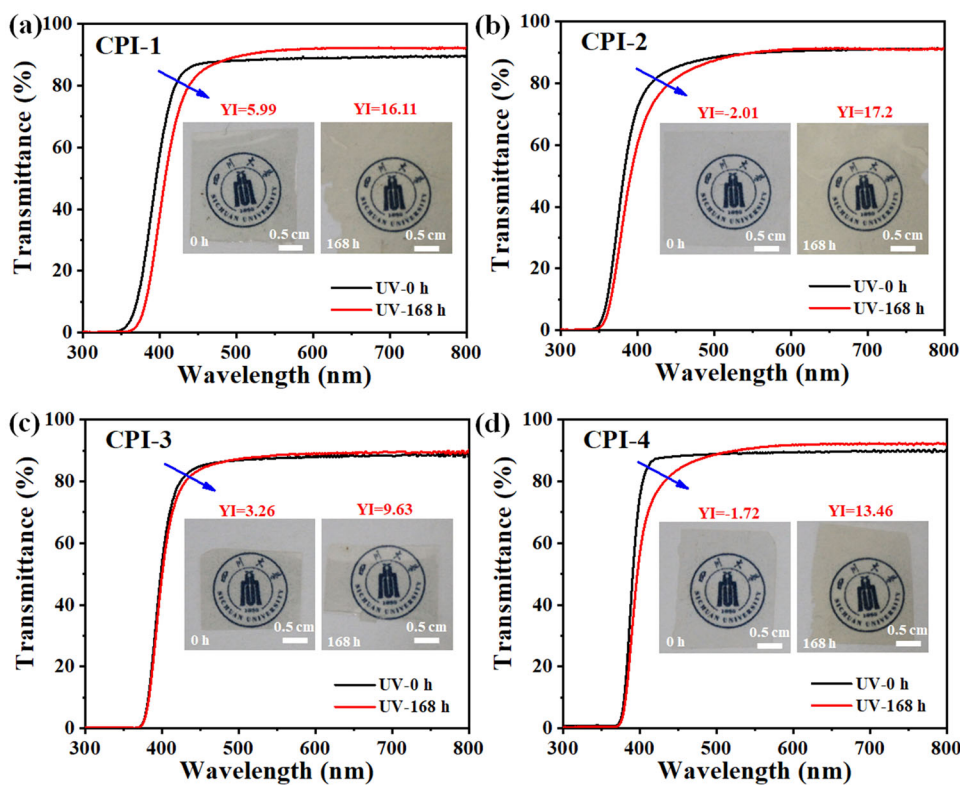


**Fig. 5** UV-Vis transmittance spectra and YI of different CPI films before and after UV irradiation. **a** CPI-1, **b** CPI-2, **c** CPI-3, and **d** CPI-4.

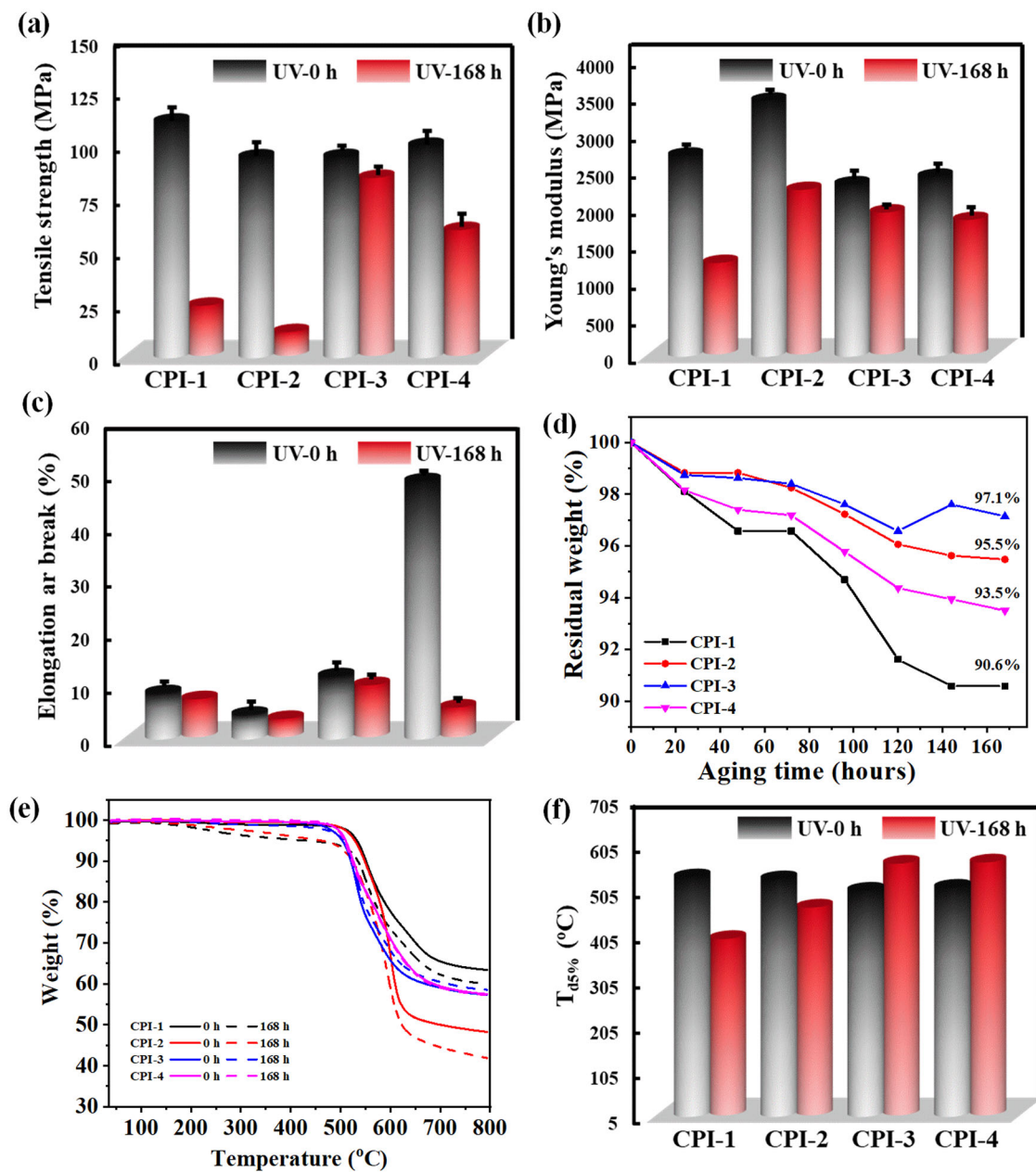
around 400 nm was observed for CPI-1, CPI-2, and CPI-4, accompanied by significant yellowing. Specifically, upon UV irradiation, YI of CPI-1, CPI-2, and CPI-4 significantly increased to 16.11, 17.2, and 13.46 respectively. In contrast, CPI-3 exhibited the most obvious resistance to yellowing, with YI of only 9.63 after being aged. The optical transparency of CPI-3 is also almost unchanged ( $T_{550\text{nm}} \sim 88\%$ ).

Figure 6 gave the changes in mechanical and thermal properties of CPI films. After UV irradiation for 168 h, the tensile strength of CPI-1 ~ CPI-4 were decreased by about 77.5, 87.3, 4.4, and 36.0%, respectively (Fig. 6a). Among them, CPI-3 showed the best mechanical integrity, which possessed the highest tensile strength of about 90 MPa after UV irradiation. A similar trend was observed for Young's modulus and elongation at break (Fig. 6b, c). Fair high retentions of 89 and 88% for Young's modulus and elongation break of CPI-3 were observed respectively after UV irradiation. The excellent UV stability of CPI-3 could be due to its peculiar conjugation structures resulting from the introduction of the fluorene unit into the molecular chain. Figure 6d showed that weight loss happened for all CPI films during UV aging, probably due to the loss of fragments on the surface and the volatilization of gaseous degradation species such as CO and  $\text{CO}_2$ <sup>46</sup>. CPI-3 exhibited the least loss of weight with a residual weight of 97.1% after UV irradiation for 168 h, while the residual weight of 90.6, 95.5, and 93.5% after UV irradiation were observed for CPI-1, CPI-2, and CPI-4 respectively. Figure 6e illustrated the thermogravimetric curves of CPI films. After UV irradiation, an obvious reduction of the thermal stability of CPI-1 and CPI-2 was observed. Specifically,  $T_{5\%}$  was decreased by 19.4 and 12.7% for CPI-1 and CPI-2 (Fig. 6f), respectively. In contrast, a minor increase of about 0.6 and 0.5% for  $T_{5\%}$  of CPI-3 and CPI-4 was observed. Overall, CPI-3 exhibited superior mechanical and thermal performance after UV irradiation.

The changes in the optical, mechanical, and thermal performance of CPI films were mainly related to the changes in the molecular structure caused by UV irradiation. We further

conducted the solubility, GPC and FTIR tests for different CPI films to understand the molecular structure changes during UV irradiation. We first conducted solubility tests for CPI films in different types of common organic solvents including Dimethylacetamide (DMAc), Dimethylformamide (DMF), and Tetrahydrofuran (THF), and the results were shown in Table 1. The solubility of CPIs was roughly classified as -, +-, and ++, which represent insoluble, partially soluble or soluble respectively at room temperature. For the fresh samples, CPI-1 and CPI-2 only can be partially soluble in different common solvents, while CPI-3 and CPI-4 were more soluble. After UV aging, all the samples showed good solubility in different solvents without any insoluble parts. These results implied that UV irradiation shall enhance the solubility of CPI films mainly by chain scission. In addition, the molecular weight distribution curves and retention percentage of  $M_w$  were shown in Fig. 7. Molecular weight distribution curves shifted to the low molecular weight part after 168 h of UV irradiation (Fig. 7a), indicating a significant decrease in molecular weight due to the breaking of the chain structure. These results were consistent with that of solubility tests. Moreover, the retention percentage of  $M_w$  of CPI-3 aged for 168 h was the highest with a value of 59%, confirming the relatively stable nature of CPI-3 (Fig. 7b).

Figure 8 gives the UV-induced evolutions in the molecular structure of different CPI films as monitored by FTIR spectra. The Pearson normalization method was used to process those spectra, following a similar procedure reported in the literature<sup>14,47</sup>. After UV irradiation, decay of peak intensity around  $1360\text{ cm}^{-1}$  assigned to the C-N bond in the imide ring was observed for all CPI films (Fig. 8a-d), without the emergence of any new characteristic peaks. The main structural change of CPI films induced by UV irradiation could be the ring opening and breakage of C-N<sup>12</sup>. Specifically, after UV aging for 168 h, the C-N index (Fig. 8e) underwent a decrease by 37, 26, 13, and 33% for CPI-1, CPI-2, CPI-3, and CPI-4, respectively. CPI-3, which contained fluorene groups



**Fig. 6 Mechanical properties, residual weight and thermal properties of different CPI films before and after UV irradiation. a** Tensile strength, **b** Young's modulus, **c** elongation at break, **d** residual weight, **e** thermogravimetric curves, and **f** initial decomposition temperature ( $T_{5\%}$ ). Error bars represent standard deviations from the results obtained at 3 replicated samples.

Table 1. Solubility of CPI films in different types of common solvents.								
	CPI-1		CPI-2		CPI-3		CPI-4	
	0 h	168 h						
DMAc	++	++	++	++	++	++	++	++
DMF	++	++	++	++	++	++	++	++
THF	++	++	++	++	++	++	++	++

++ Soluble at room temperature, +- partially soluble or swelling, - insoluble.

and C-O-C bonds, experienced the least chain breakage and the best UV resistance. In addition, the evolution of C=O bonds was also monitored (Fig. 8f). It shall be noted that different from C-N bonds, both the formation and depletion of C=O bonds could happen during the oxidation and degradation of CPI film<sup>11,14</sup>. After UV aging, reduction in the content of C=O bonds were actually observed for all CPI films, which indicating that the depletion of C=O bonds could be dominated. Taken together, the FTIR results showed that chain scission mainly happened for all CPI films during UV irradiation, which supplemented the observations from solubility and GPC tests. The typical degradation mechanism of CPI films for the deterioration of mechanical and optical

properties can be deduced and summarized in Fig. 8g. Under ultraviolet irradiation, ring opening shall happen and the C-N bond in polyimide can be broken and combined with oxygen, giving free radicals and volatile products such as alkane gas,  $\text{CO}_2$ , etc. Those chain scission mechanisms shall be responsible for the deterioration of the thermal or mechanical properties of CPI films<sup>48,49</sup>.

We further built a pentagonal radar chart to visually compare the key structure and performance of CPI films after UV aging, as shown in Fig. 9. Upon UV irradiation, the retention of the C-N bond of CPI-3 films was higher than that of other CPI films, indicating its least chain scission. Moreover, the tensile strength and elongation at break of CPI films were the highest after UV irradiation. In contrast, CPI-1 and CPI-2 underwent a severe degradation in the

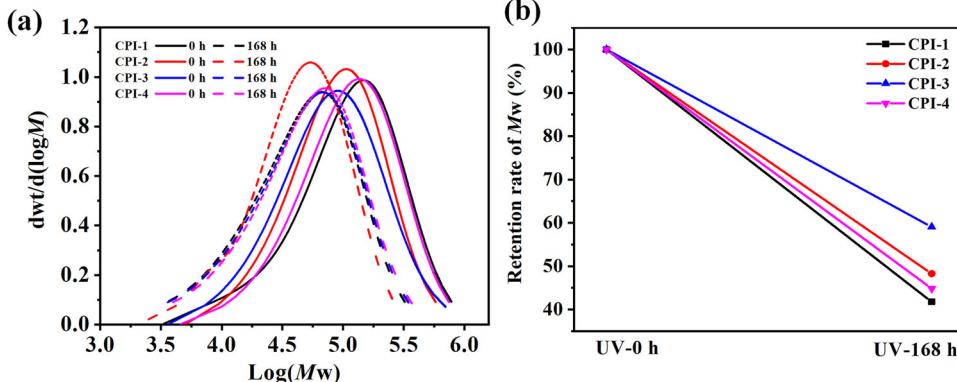


**Fig. 7 Evolution in molecular structures of CPI films before and after UV irradiation. a** Molecular weight distribution curves, **b** retention rate of  $M_w$ .

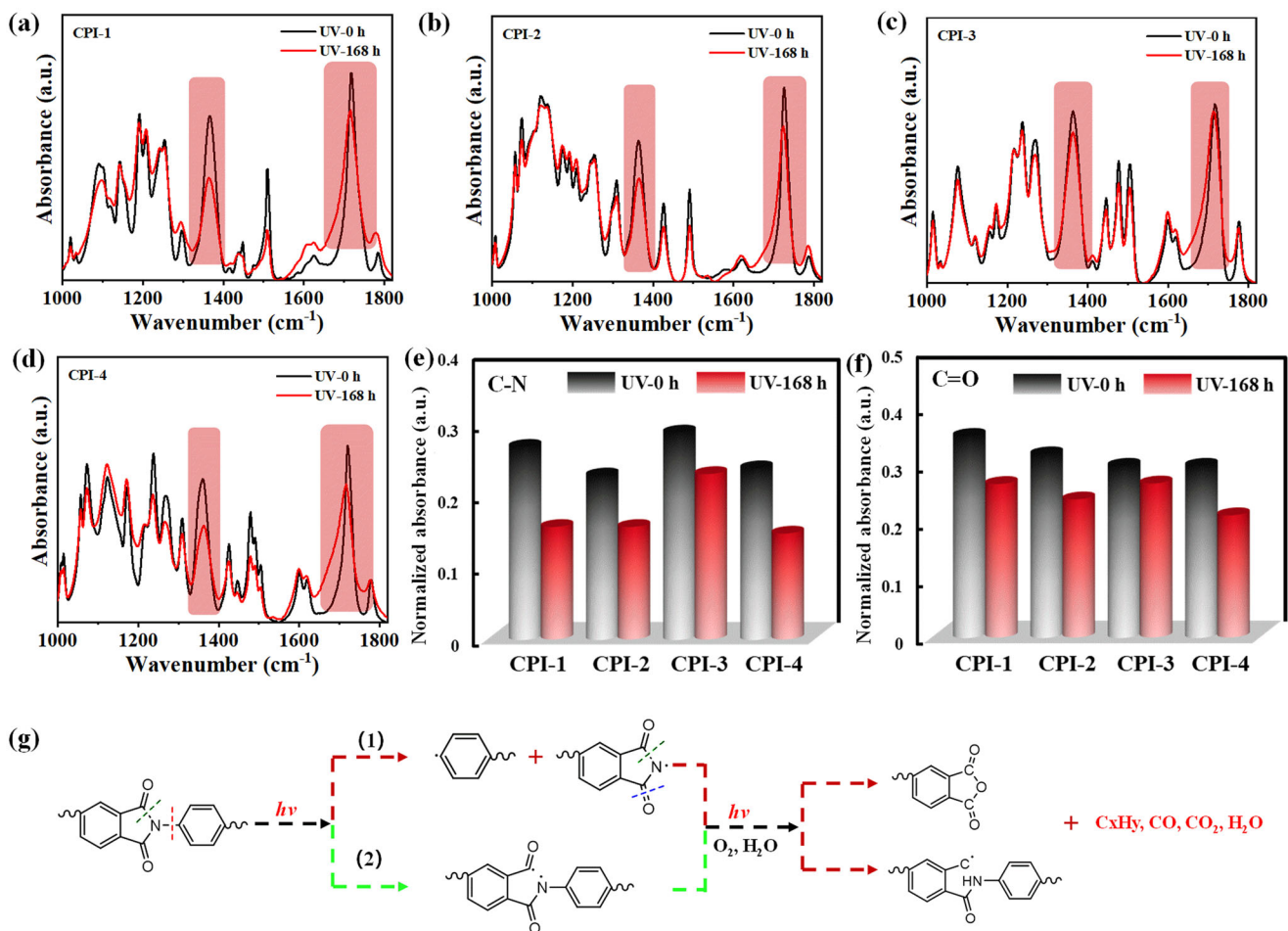


**Fig. 8 Chemical structures and possible degradation mechanisms of CPI films.** Normalized FTIR spectra of **a** CPI-1, **b** CPI-2, **c** CPI-3, **d** CPI-4, as well as **e** absorbance of C-N bond and **f** absorbance of C=O bond before and after UV irradiation, **g** possible changes in the molecular structure of CPI films upon UV irradiation: chain scission and formation of volatile small molecules.

mechanical properties during UV aging, due to the breakage of the C-N and C=O bond as well as the opening of the imide ring<sup>46</sup>. In addition, poor thermal stability and significant discoloration were also observed in CPI-1, CPI-2, and CPI-4 films after UV irradiation, while CPI-3 maintained its high thermal stability and low discoloration with  $T_{5\%}$  of 506 °C and YI of 9.63. Overall, the introduction of fluorene and the strong conjugation effect made the molecular chains of CPI-3 interact with each other more strongly, leading to its excellent UV resistance.

To further reveal the UV resistance mechanisms of CPI-3, the potential UV energy dissipation paths for CPI-3 were explored. In general, the polymer molecular chain was excited after absorbing UV energy and jumps from the stable ground state ( $S_0$ ) to the high-energy excited state ( $S_1$ ), as shown in Fig. 10a. The atoms in the excited state were generally unstable<sup>45,50–53</sup>, as a result, the UV stability of the material was mainly determined by whether the excited molecules can return to their original state by efficiently harmlessly dissipating the absorbed energy. In this regard, energy dissipation in the form of fluorescence or thermal radiation was preferred, both of which have been found to work for CPI-3.

The first dissipation path, which is the release of energy through fluorescence radiation, was shown in Fig. 10b. Under near-UV

wavelength excitation at 405 nm, only relatively low fluorescence emission was observed for CPI-1 (maximum fluorescence intensity of 32.3), CPI-2 (29.3), and CPI-4 (90.5), which could be due to the presence of trifluoromethyl<sup>54</sup>. However, CPI-3, which contained fluorene, isopropylidene, and ether groups, showed a very strong fluorescence emission (157.2), probably due to the increased density of aromatic rings in the molecular chain and contributed to the conjugation in the polyimide molecular structure, enhancing the  $\pi-\pi^*$  leap of the molecule<sup>55,56</sup>. It has been reported that the existence of an isopropylidene group or ether group could enhance the fluorescence emission ability of CPIs. For example, Wu et al.<sup>57</sup> found that PIs containing the isopropylidene group exhibited higher fluorescence intensity (approximately 5000 a.u.) compared to OH-6FDA containing the trifluoromethyl group (approximately 1000 a.u.). In addition, the interchain interactions could also contribute to the higher fluorescence emission of CPI-3<sup>28</sup>. The path of the thermal radiation mechanism was further verified by infrared thermography. The thermal images of CPI films were taken under UV radiation at a wavelength of 365 nm, as shown in Fig. 10c. The maximum temperatures of CPI-1 to CPI-4 were 34.3, 32.8, 42.1, and 38 °C, respectively. The heat release could be due to the vibration, rotation, and motion of atoms and molecules induced by higher energy<sup>58</sup>, or the out-of-plane deformation of ring centers, mutual isomerization<sup>50</sup>, etc. CPI-3 exhibited the highest radiation temperature, which demonstrated that thermal radiation was another effective way for the dissipation of UV energy.

Furthermore, the UV resistance of CPI-3 was also compared with that of traditional yellow PI film, which mainly consisted of pyromellitic anhydride (PMDA) and 4,4'-Oxydianiline (ODA). The evolution in tensile strength and onset decomposition temperature of the traditional yellow PI film (PMDA-ODA) and CPI-3 (BPADA-BAPF) during UV aging were studied for up to 336 h (Fig. 11). The tensile strength of both CPI-3 and traditional yellow PI were decreased gradually over aging time. For example, the tensile strength of fresh traditional yellow PI was decreased from  $132.2 \pm 3.3$  MPa to  $108.6 \pm 10.5$  MPa by 18% after 336 h, while was decreased from  $94.6 \pm 12.5$  MPa to  $45.1 \pm 3.0$  MPa by 52% for CPI-3. In addition, after 336 h of UV aging, only a minor reduction in  $T_{5\%}$  was observed for both traditional yellow PI and CPI-3. Taken together, these results indicated that CPI-3 showed decent UV

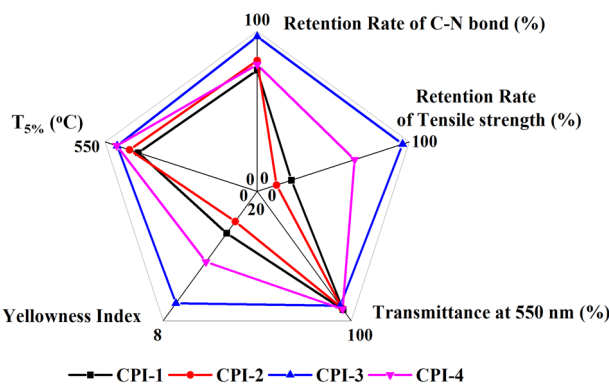


**Fig. 9** Pentagonal radar chart for the comparison of comprehensive performance of different CPI films after UV irradiation.

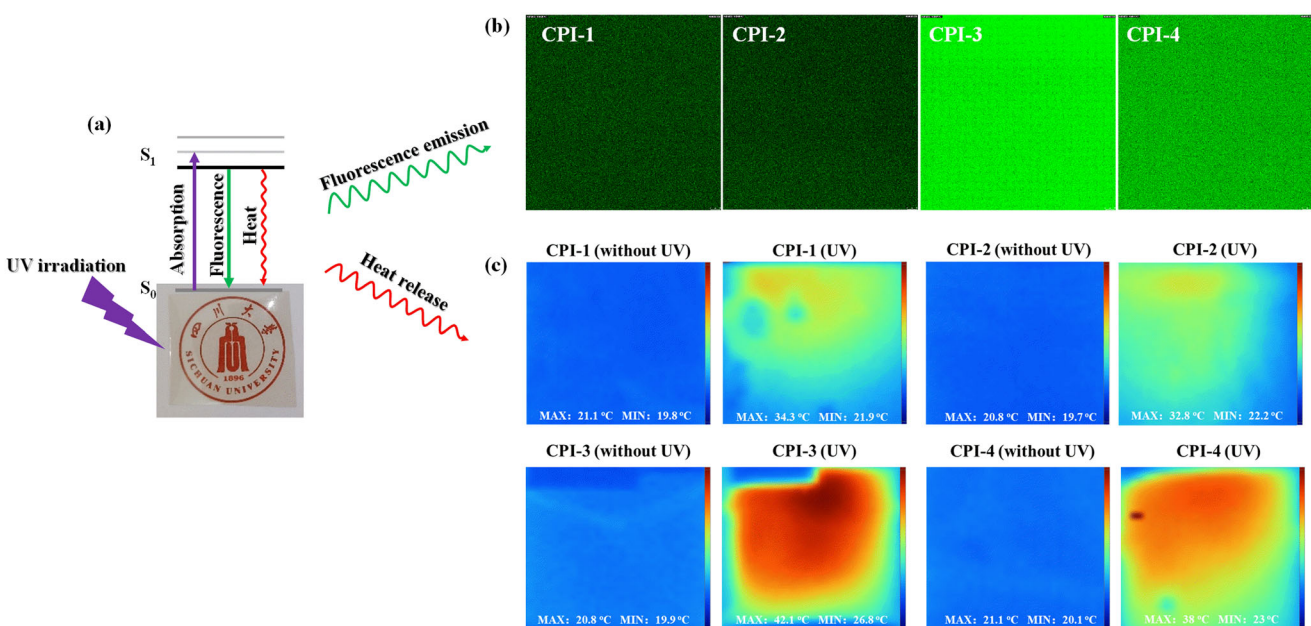


**Fig. 10** UV dissipation of different CPI films. **a** Scheme of UV absorption and energy dissipation of CPI films, **b** fluorescence images, and **c** infrared thermal images.

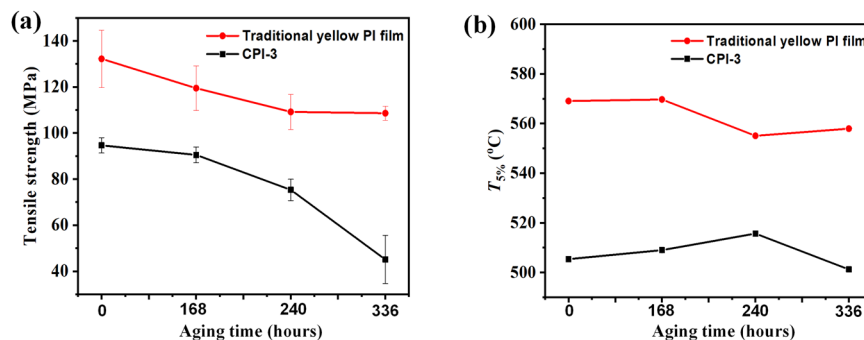


**Fig. 11 Comparison of UV resistance between traditional yellow film and CPI-3 film over aging time. a** Tensile strength and **b** onset decomposition temperature of. Error bars represent standard deviations from the results obtained at 3 replicated samples.

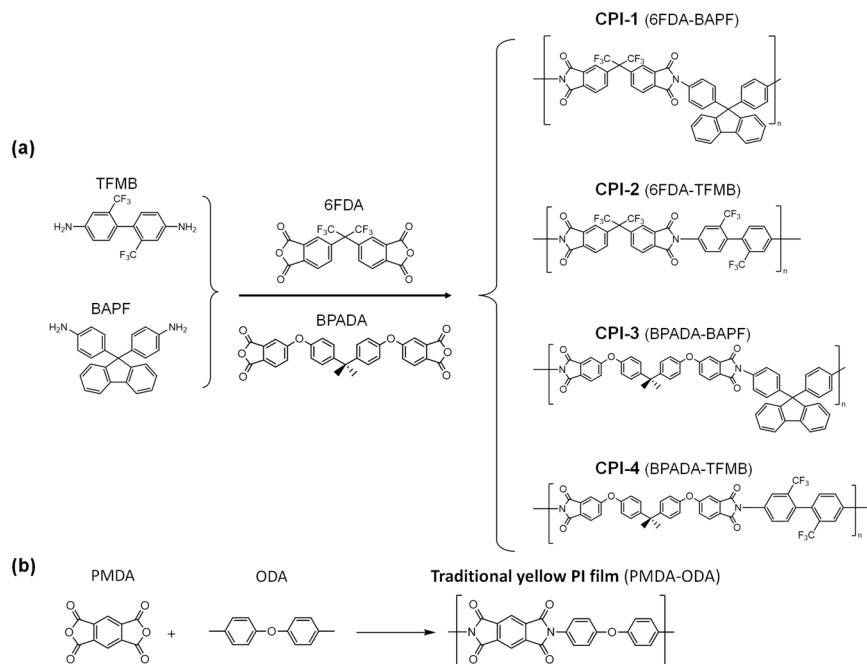


**Fig. 12 Synthetic routes and nomination for different polyimide films. a** 4 types of CPIs and **b** traditional yellow PI film.

resistance at an extended aging time, even though it was slightly inferior to that of traditional yellow PI film.

In this work, a series of CPI films with different charge transfer interactions were synthesized by introducing trifluoromethylene, fluorene, or ether bonds. The relationship between their structures and UV resistance as well as optical properties and mechanical properties etc. were explored. It was found that the simultaneous introduction of trifluoromethylene and fluorene significantly improved the optical transparency, thermal stability, and mechanical strength of CPI films. Moreover, the introduction of trifluoromethylene and flexible ether bonds effectively improved the optical transparency and toughness. Note that the existence of isopropylidene, ethers and fluorenes effectively endowed CPI film (CPI-3) with optimal UV resistance and decent initial performance (optical transparency, thermal stability, and toughness) simultaneously. Specifically, after being subjected to high-intensity UV irradiation, CPI-3 not only maintained over 90% of its mechanical properties but also retained its high optical properties ( $T_{550\text{nm}} \sim 88\%$ ) and thermal stability ( $T_{5\%} \sim 506^\circ\text{C}$ ). The UV stability of CPI-3 was attributed to its efficient dissipation ability of absorbed UV energy via the routes of both fluorescence emission

and photothermal conversion. The optimized comprehensive performance of CPI-3 could be related to its sophisticated charge transfer interaction in the conjugation structure. The design strategy paved the way for optimizing the durability of polyimides for energy conversion and electronic applications resisting harsh conditions.

## METHODS

### Materials

4,4'-(Hexafluoroisopropylidene)diphthalic Anhydride (6FDA), 4,4'-(4,4'-Isopropylidenediphenoxyl)diphthalic Anhydride (BPADA), 9,9-Bis(4-aminophenyl)fluorene (BAPF), and 2,2'-Bis(trifluoromethyl)benzidine (TFMB) were purchased from Shanghai Macklin Biochemical Technology Co., Ltd. Anhydrous N,N-Dimethylacetamide (DMAc) were purchased from Shanghai Aladdin Biochemical Technology Co., Ltd, while anhydrous ethanol, acetic anhydride, and pyridine were purchased from Chengdu Cologne Chemical Co., Ltd. All monomers were carefully dried before any use.

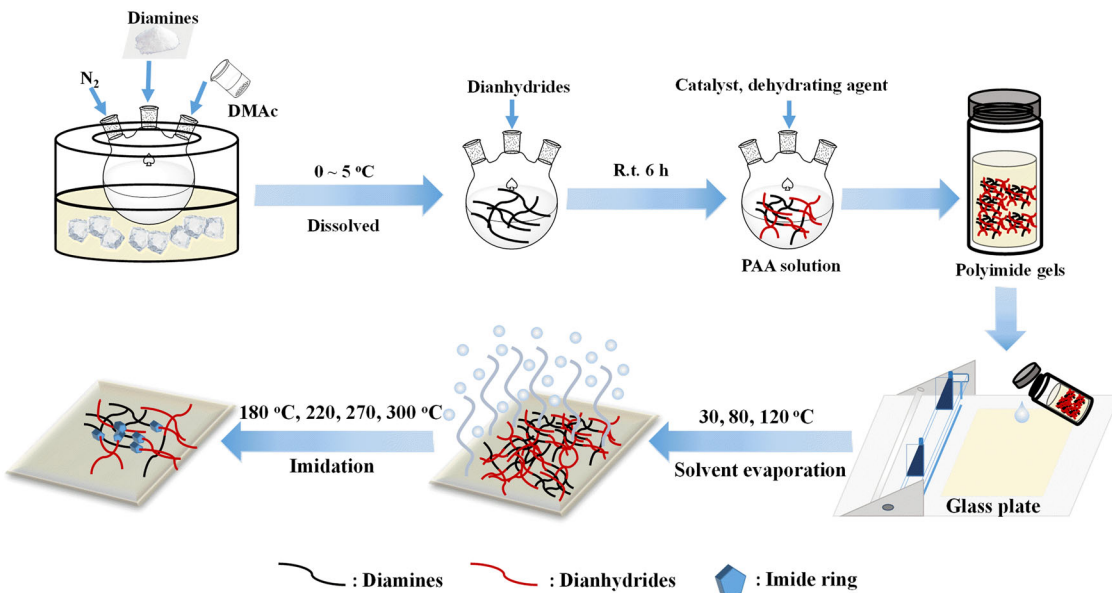


**Fig. 13** Schematic for the fabrication process of CPI films and traditional yellow PI film.

### Synthesis and fabrication of Polyimide (PIs) films

A series of aromatic polyimides (CPIs) were synthesized by introducing trifluoromethyl, fluorene, or ether groups, including 6FDA-BAPF (CPI-1), 6FDA-TFMB (CPI-2), BPADA-BAPF (CPI-3), and BPADA-TFMB (CPI-4), as shown in Fig. 12a. A general procedure for the fabrication of CPIs was illustrated by the synthesis of CPI-3 (Fig. 13). First, BAPF (1.74 g, 5 mmol) and anhydrous DMAc (17.5 ml, 20 wt%) were added into a 50 mL flask, stirring for 20 min under a nitrogen atmosphere to completely dissolve. 6FDA (2.628 g, 5.05 mmol) was then added into the above mixture solution in three batches. The mixture solution was stirred at room temperature for 8 h to obtain a transparent polyamic acid (PAA). In the process of chemical imidization, pyridine needed to be added as a catalyst and acetic anhydride as a dehydrating agent, and finally, a polyimide glue solution was obtained. The PAA solution was coated on a 10 cm × 10 cm glass plate by an experimental coater (MS-ZN320B, Xiamen, China), and then placed in an oven for high-temperature imidization. The PAA solution was dried at 30, 80, and 120 °C for 2 h, respectively, to remove most of the solvent slowly without the formation of bubbles, and to start a pre-imidization process. Then it was imidized at 180, 220, 270, and 300 °C for 1 h, respectively to complete the imidization process. Finally, the colorless polyimide (CPI) films with a thickness of around 30 μm were successfully synthesized by adjusting the appropriate solid content. For comparison, traditional yellow PI film consisted of pyromellitic anhydride (PMDA) and 4,4'-Oxydianiline (ODA) were also synthesized following a similar procedure (Fig. 12b).

### UV aging test

CPI films were cut into 5 cm × 5 cm squares and loaded in a homemade photo-oxidation aging apparatus with an iodine-gallium lamp (500 W) and a temperature-control system (Fig. 14). The direct distance between the film and the iodine-gallium lamp was controlled to be 30 cm. The exposure intensity was  $10 \pm 3 \text{ W m}^{-2}$  measured by a UV-A luminometer (Beijing Normal University Photoelectric Instrument Factory) and the temperature was constant at  $30 \pm 1 \text{ }^{\circ}\text{C}$ . The maximum intensity of the UV exposure was 365 nm. Samples were collected regularly for the characterization of structure and properties.

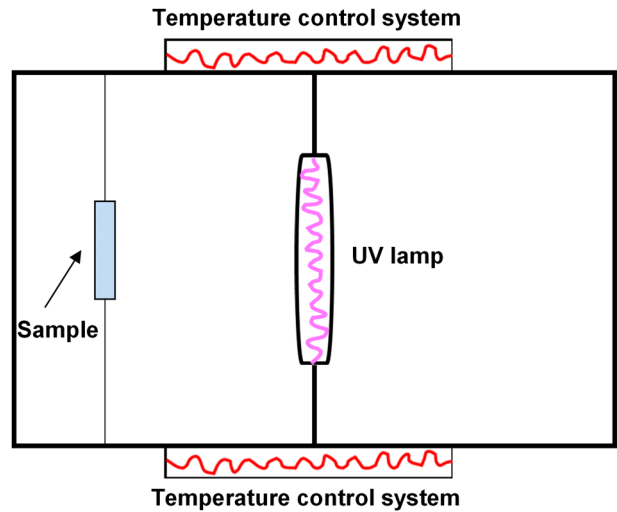


**Fig. 14** Schematic for the homemade photo-oxidation aging apparatus.

### Characterizations

**Chemical structures.** FTIR spectra were obtained by testing polyimide films on a Nicolet 6700 (Thermo Fisher Scientific) spectrometer in attenuated total reflectance mode with a resolution of  $4 \text{ cm}^{-1}$  and 32 scans in the region between 650 and  $4000 \text{ cm}^{-1}$ . Infrared spectra were normalized by spectral area from 650 to  $2000 \text{ cm}^{-1}$  to analyze the changes in group content during aging<sup>14,47</sup>. The C–N and C=O functional group indices were calculated by intensity of the normalized C–N and C=O bond peak, respectively.  $^1\text{H-NMR}$  and  $^{13}\text{C-NMR}$  spectra were conducted on a Bruker 400 M apparatus, in which all CPI films were dissolved in N,N-Dimethylformamide-d<sup>7</sup> (DMF-d<sup>7</sup>). The crystalline properties of CPI films were measured by a Smart Lab XRD (Rigaku Co., Japan). The copper target was selected for testing, with a scanning range of 5~90° and a scanning speed of  $2^{\circ} \text{ min}^{-1}$ . The average molecular mass was measured by an HLC8320 GPC (Tosoh Co., Tokyo, Japan). DMF was used as the mobile phase, the test temperature was

room temperature, polystyrene was selected as the standard sample, the injected sample volume was 10  $\mu\text{L}$ , and the running time was 15 min. The solubility test was characterized by cutting various CPI films into 10 mg at room temperature (25 °C) and dissolving them in different aprotic solvents for 24 h.

**Calculation of quantum chemistry.** To understand the conjugation effects in molecules, the energy levels of the molecular orbits of CPI films were calculated by density functional theory (DFT) / B3LYP/6-311G(d, p) with the Gaussian 16 program package<sup>59</sup>. Gaussian 16 was used to optimize and analyze the frequency of four initial structures. B3LYP was used as the function and 6-31 g(d) was used as the basis set. Subsequently, the molecular orbital analysis of molecular structure was carried out by GaussView 6.0.

**Optical properties.** The transmittance of the CPI films was measured in the wavelength range of 200–800 nm by using the Lambda 750 S UV-VIS-NIR spectrum of PerkinElmer. In addition, the CIE index and yellowness index (YI) were measured using a spectrophotometer (TS7020, 3nh®), following ASTM E 313-20. Measurements were taken using a D65 standard illuminant and a 10-degree observer in a planar viewing mode. For optical testing, CPI films with a size of 10 × 10 cm were used, and five points were selected for testing. ASTM E 313-20:

$$\text{YI} = 100(1.3013X - 1.1498Z)/Y \quad (1)$$

where X, Y, and Z were the measured tristimulus values.

**Thermal and mechanical properties.** To probe the thermal behaviors of CPI films, thermogravimetric analysis (TGA) was performed under a nitrogen atmosphere by using TGA 550 (TA Instrument, USA). The temperature was increased from 25 to 800 °C at a heating rate of 10 °C min<sup>-1</sup>. Before tests, CPI films were dried in an oven to avoid the effect of moisture on tests. Dynamic thermomechanical analysis (DMA) was carried out on a Q850 (TA Instruments, USA) in the tensile mode. The temperature ranged from –30 to 400 °C, with a heating rate of 5 °C min<sup>-1</sup>, a frequency of 1 Hz, and an amplitude of 10  $\mu\text{m}$ . For CPI-1 to CPI-4, samples with dimensions of 6 × 6 mm × 30  $\mu\text{m}$  were used. Mechanical properties of CPI films were obtained on a universal mechanical testing machine (INSTRON 5967, USA) with a speed of 5 mm s<sup>-1</sup> and a gauge length of 15 mm. CPI films with the dimensions of 6 × 35 mm rectangles were used. At least five replicated samples were measured.

Fluorescence imaging was performed using a Leica SP8 laser scanning confocal microscope (Leica Microscopy, Wetzlar, Germany) with a near-UV excitation wavelength of 405 nm. IR thermographic images of the CPI films were taken using a FLUKE Ti32S thermal imager (Fluke Infrared Camera, Shanghai, China) at a wavelength of 365 nm with an 80 W high-power UV LED light.

## DATA AVAILABILITY

All data generated or analyzed during this study are included in this published article and any additional data that support the findings of this study are available from the corresponding author upon reasonable request.

Received: 10 August 2023; Accepted: 26 December 2023;

Published online: 11 January 2024

## REFERENCES

- Constantin, C.-P. & Damaceanu, M.-D. A refreshing perspective on electrochromic materials: Phenoxazine as an opportune moiety towards stable and efficient electrochromic polyimides. *Chem. Eng. J.* **465**, 142883 (2023).
- Wu, Y., Ji, J., Huang, H., Liu, S. & Zhao, J. Facile synthesis of acyloxy-containing fluorene-based cardo polyimides with high optical transparency, fluorescence and low dielectric constant. *React. Funct. Polym.* **166**, 104979 (2021).
- Gouzman, I. et al. Advances in polyimide-based materials for space applications. *Adv. Mater.* **31**, 1807738 (2019).
- Wu, C.-C. Ultra-high transparent sandwich structure with a silicon dioxide passivation layer prepared on a colorless polyimide substrate for a flexible capacitive touch screen panel. *Sol. Energy Mater. Sol. Cells* **207**, 110350 (2020).
- Yoon, J. et al. Foldable perovskite solar cells using carbon nanotube-embedded ultrathin polyimide conductor. *Adv. Sci.* **8**, 2004092 (2021).
- Wang, Y. et al. Polyimide/ZnO composite cooperatively crosslinked by Zn<sup>2+</sup> Salt-Bondings and hydrogen bondings for ultraflexible organic solar cells. *Chem. Eng. J.* **451**, 138612 (2023).
- Ni, H.-J., Liu, J.-G., Wang, Z.-H. & Yang, S.-Y. A review on colorless and optically transparent polyimide films: chemistry, process and engineering applications. *J. Ind. Eng. Chem.* **28**, 16–27 (2015).
- Zhao, X., Geng, Q.-F., Zhou, T.-H., Gao, X.-H. & Liu, G. Synthesis and characterization of novel polyimides derived from unsymmetrical diamine: 2-amino-5-[4-(2'-aminophenoxy) phenyl]-thiazole. *Chin. Chem. Lett.* **24**, 31–33 (2013).
- Tu, F. et al. Photoinduced radical persistent luminescence in semialiphatic polyimide system with temperature and humidity resistance. *Adv. Sci.* **10**, 2301017 (2023).
- Lai, S. et al. Highly soluble fluorinated polyimides with promising gas transport performance and optical transparency. *Polym. Chem.* **14**, 359–373 (2023).
- Feng, J. et al. Revealing molecular mechanisms of colorless transparent polyimide films under photo-oxidation. *Polym. Degrad. Stab.* **210**, 110294 (2023).
- Feng, J. et al. Property evolution and molecular mechanisms of aluminalized colorless transparent polyimide under space ultraviolet irradiation. *Polym. Degrad. Stab.* **199**, 109915 (2022).
- Hoyle, C. E. & Anzures, E. T. Photodegradation of polyimides. I. A spectral, viscometric, chromatographic, and weight loss investigation of polyimides based on a hexafluorinated dianhydride. *J. Appl. Polym. Sci.* **43**, 1–10 (1991).
- Mai, A. T. M. et al. Photodegradation of a semi-aromatic bio-derived polyimide. *Polym. Degrad. Stab.* **184**, 109472 (2021).
- Song, D. et al. Soluble and colorless polyimide coated cotton fabric with attractive multifunction: warmth retention, breathable, antifouling, UV and acid resistance. *Chem. Eng. J.* **455**, 140755 (2023).
- Tanaka, T., Bando, K. K., Matsubayashi, N., Imamura, M. & Shimada, H. Comparison of photo-degradation of polyimide film by UV irradiation in air and in vacuum. *Phys. Scr.* **2005**, 412 (2005).
- Wei, X. Y. et al. Enhancement of ultraviolet light resistance of colorless and transparent semi-alicyclic polyimide nanocomposite films via the incorporation of hindered amine light stabilizers for potential applications in flexible optoelectronics. *Polymers* **14**, 1091 (2022).
- Kim, S., Hwang, T. G., Namgoong, J. W., Kim, H. M. & Kim, J. P. Effect of linker moiety on linear dimeric benzotriazole derivatives as highly stable UV absorber for transparent polyimide film. *Dyes Pigm* **180**, 108469 (2020).
- Harito, C., Bavykin, D. V., Yuiliarto, B., Dipojono, H. K. & Walsh, F. C. Inhibition of polyimide photodegradation by incorporation of titanate nanotubes into a composite. *J. Polym. Environ.* **27**, 1505–1515 (2019).
- Pavlenko, V. I. & Cherkashina, N. I. Effect of SiO<sub>2</sub> crystal structure on the stability of polymer composites exposed to vacuum ultraviolet radiation. *Acta Astronaut* **155**, 1–9 (2019).
- Hu, L., Li, M., Xu, C., Luo, Y. & Zhou, Y. A polysilazane coating protecting polyimide from atomic oxygen and vacuum ultraviolet radiation erosion. *Surf. Coat. Technol.* **203**, 3338–3343 (2009).
- Kimoto, Y., Fujita, T., Furuta, N., Kitamura, A. & Suzuki, H. Development of space-qualified photocurable-silsesquioxane-coated polyimide films. *J. Spacecr. Rockets* **53**, 1028–1034 (2016).
- Lu, Y. et al. Preparation and properties of in situ amino-functionalized graphene oxide/polyimide composite films. *Appl. Surf. Sci.* **422**, 710–719 (2017).
- He, T. et al. Direct fluorination as a one-step ATRP initiator immobilization for convenient surface grafting of phenyl ring-containing substrates. *Polym. Chem.* **11**, 5693–5700 (2020).
- Zhang, L. et al. Hydroxyl-functionalized block co-polyimide enables simultaneously improved toughness and strength of tetrafunctional epoxy resin. *Compos. Sci. Technol.* **230**, 109787 (2022).
- Sun, H. et al. Cardo polyimides/TiO<sub>2</sub> mixed matrix membranes: synthesis, characterization, and gas separation property improvement. *Sep. Purif. Technol.* **122**, 367–375 (2014).
- Li, L., Xu, Y., Che, J., Su, X. & Song, C. Transparent fluorinated poly(imide siloxane) copolymers with good adhesivity. *Macromol. Res.* **25**, 1076–1084 (2017).
- Abe, A. et al. Theoretical and experimental studies on the mechanism of coloration of polyimides. *ChemPhysChem* **12**, 1367–1377 (2011).
- Liu, Y. Y., Wang, Y. K. & Wu, D. Y. Synthetic strategies for highly transparent and colorless polyimide film. *J. Appl. Polym. Sci.* **139**, e52604 (2022).

30. Wu, Q., Ma, X., Zheng, F., Lu, X. & Lu, Q. High performance transparent polyimides by controlling steric hindrance of methyl side groups. *Eur. Polym. J.* **120**, 109235 (2019).
31. Li, X. et al. Colorless polyimide films with low birefringence and retardation: synthesis and characterization. *Polymer* **265**, 125579 (2023).
32. Bao, F. et al. Colorless polyimides derived from rigid trifluoromethyl-substituted triphenylenediamines. *Polymer* **273**, 125883 (2023).
33. Xiao, P., He, X., Zheng, F. & Lu, Q. Super-heat resistant, transparent and low dielectric polyimides based on spirocyclic bisbenzoxazole diamines with  $T_g > 450^\circ\text{C}$ . *Polym. Chem.* **13**, 3660–3669 (2022).
34. Shen, J. et al. Soluble sulfoxide biphenyl polyimide film with transmittance exceeding 90%. *Polymer* **254**, 125050 (2022).
35. Kim, J. W. & Chang, J.-H. Syntheses of colorless and transparent polyimide membranes for microfiltration. *Polymers* **12**, 1610 (2020).
36. Shu, M. et al. Surface modification of poly(4,4'-oxydiphenylene pyromellitimide) (Kapton) by alkali solution and its applications to atomic oxygen protective coating. *Corros. Sci.* **112**, 418–425 (2016).
37. Zuo, H.-T. et al. Highly transparent and colorless polyimide film with low dielectric constant by introducing meta-substituted structure and trifluoromethyl groups. *Chin. J. Polym. Sci.* **39**, 455–464 (2021).
38. Hsiao, S.-H., Guo, W., Tsai, T.-H. & Chiu, Y.-T. Synthesis of soluble and thermally stable triptycene-based poly(amide-imide)s. *J. Polym. Res.* **21**, 1–10 (2014).
39. Gao, H., Li, J., Xie, F., Liu, Y. & Leng, J. A novel low colored and transparent shape memory copolyimide and its durability in space thermal cycling environments. *Polym. Chem.* **156**, 121–127 (2018).
40. Su, C. et al. High-transparency and colorless polyimide film prepared by inhibiting the formation of chromophores. *Polymers* **14**, 4242 (2022).
41. Zhang, L. et al. Dielectric property and charge evolution behavior in thermally aged polyimide films. *Polym. Degrad. Stab.* **156**, 292–300 (2018).
42. Li, G., Zhuo, W.-Y., Yang, G., Niu, Y.-H. & Li, G.-X. J. A. P. S. Study on the aging behaviors and mechanism of nitrile rubber under multiple coupled factors. *Acta Polym. Sin.* **52**, 762–774 (2021).
43. Chen, H. et al. Polyimides containing a novel bisbenzoxazole with high  $T_g$  and low CTE. *RSC Adv.* **11**, 16924–16930 (2021).
44. Luo, S. et al. Finely tuning the free volume architecture in iptycene-containing polyimides for highly selective and fast hydrogen transport. *Macromolecules* **49**, 3395–3405 (2016).
45. Hu, G. et al. Synthesis of silicon quantum dots with highly efficient full-band UV absorption and their applications in antiyellowing and resistance of photo-degradation. *ACS Appl. Mater. Interfaces* **11**, 6634–6643 (2019).
46. Sang, T., Wallis, C. J., Hill, G. & Britovsek, G. J. Polyethylene terephthalate degradation under natural and accelerated weathering conditions. *Eur. Polym. J.* **136**, 109873 (2020).
47. Dao, A. T., Nakayama, K., Shimokata, J. I. & Taniike, T. Multilateral characterization of recombinant spider silk in thermal degradation. *Polym. Chem.* **8**, 1049–1060 (2017).
48. Rosu, L., Sava, I. & Rosu, D. Modification of the surface properties of a polyimide film during irradiation with polychromatic light. *Appl. Surf. Sci.* **257**, 6996–7002 (2011).
49. Yokota, K., Ohmae, N. & Tagawa, M. Effect of relative intensity of 5 eV atomic oxygen and 172 nm vacuum ultraviolet in the synergism of polyimide erosion. *High. Perform. Polym.* **16**, 221–234 (2004).
50. Lyu, Y., Gu, X. & Mao, Y. Green composite of instant coffee and poly(vinyl alcohol): an excellent transparent UV-shielding material with superior thermal-oxidative stability. *Ind. Eng. Chem. Res.* **59**, 8640–8648 (2020).
51. Kirkbright, G., Narayanaswamy, R. & West, T. The fluorescence and phosphorescence characteristics of some antioxidants and ultraviolet absorbers. *Anal. Chim. Acta* **52**, 237–246 (1970).
52. Louis, M. et al. Blue-light-absorbing thin films showing ultralong room-temperature phosphorescence. *Adv. Mater.* **31**, 1807887 (2019).
53. Rosales, S. A., González, F., Moreno, F. & Gutiérrez, Y. Non-absorbing dielectric materials for surface-enhanced spectroscopies and chiral sensing in the UV. *Nanomaterials* **10**, 2078 (2020).
54. Ward, J. S. et al. Exploiting trifluoromethyl substituents for tuning orbital character of singlet and triplet states to increase the rate of thermally activated delayed fluorescence. *Mater. Chem. Front.* **4**, 3602–3615 (2020).
55. Wakita, J., Sekino, H., Sakai, K., Urano, Y. & Ando, S. Molecular design, synthesis, and properties of highly fluorescent polyimides. *J. Phys. Chem. B* **113**, 15212–15224 (2009).
56. Wu, Y. et al. Multifunctional polyimides by direct silyl ether reaction of pendant hydroxy groups: Toward low dielectric constant, high optical transparency and fluorescence. *Eur. Polym. J.* **132**, 109742 (2020).
57. Wu, Y., Liu, S. & Zhao, J. Simultaneously improving the optical, dielectric, and solubility properties of fluorene-based polyimide with silyl ether side groups. *ACS Omega* **7**, 11939–11945 (2022).
58. Li, J. et al. Two distinctive energy migration pathways of monolayer molecules on metal nanoparticle surfaces. *Nat. Commun.* **7**, 10749 (2016).
59. Frisch, M. J. et al. *Gaussian 16, Revision C.01*. (Gaussian Inc., Wallingford, CT, 2016).

## ACKNOWLEDGEMENTS

The authors are grateful for the financial support from the National Natural Science Foundation of China (U19A2096, 52003175), Department of Science and Technology of Sichuan Province under grant number of 2022NSFSC2012, the Fundamental Research Funds for the Central Universities.

## AUTHOR CONTRIBUTIONS

L.X.: Investigation, writing original draft & editing. Y.L.: Conceptualization, Project administration, Writing - review & editing. J.F.: Writing - review & editing. Yanyan.H.: Writing - review & editing. Yajiang.H.: Writing - review & editing. Q.Y.: Writing - review & editing. G.L.: Writing - review & editing. M.K.: Conceptualization, Funding acquisition, Writing - review & editing.

## COMPETING INTERESTS

The authors declare no competing interests.

## ADDITIONAL INFORMATION

**Correspondence** and requests for materials should be addressed to Yadong Lv or Miqui Kong.

**Reprints and permission information** is available at <http://www.nature.com/reprints>

**Publisher's note** Springer Nature remains neutral with regard to jurisdictional claims in published maps and institutional affiliations.



**Open Access** This article is licensed under a Creative Commons Attribution 4.0 International License, which permits use, sharing, adaptation, distribution and reproduction in any medium or format, as long as you give appropriate credit to the original author(s) and the source, provide a link to the Creative Commons license, and indicate if changes were made. The images or other third party material in this article are included in the article's Creative Commons license, unless indicated otherwise in a credit line to the material. If material is not included in the article's Creative Commons license and your intended use is not permitted by statutory regulation or exceeds the permitted use, you will need to obtain permission directly from the copyright holder. To view a copy of this license, visit <http://creativecommons.org/licenses/by/4.0/>.

© The Author(s) 2024